ELSEVIER

Wave Motion 35 (2002) 17–40

WAVE MOTION

www.elsevier.com/locate/wavemoti

A 2D hypersingular time-domain traction BEM for transient elastodynamic crack analysis☆

Ch. Zhang*

Department of Civil Engineering, University of Applied Sciences, Hochschule Zittau/Görlitz, D-02763 Zittau, Germany

Received 30 August 2000; accepted 1 December 2000

Abstract

A two-dimensional (2D) hypersingular time-domain traction BEM for transient elastodynamic crack analysis is presented in this paper. Time-domain traction boundary integral equations (BIEs) are applied for this purpose, to both crack-faces and external boundaries of the cracked solid. A numerical solution procedure is developed for solving the hypersingular time-domain traction BIEs. A time-stepping scheme in conjunction with a collocation method is applied. The time-stepping scheme uses a linear temporal shape-function which makes an analytical time-integration of the convolution integrals possible. As spatial shape-functions, two different shape-functions are adopted: a square-root crack-tip shape-function for elements adjacent to crack-tips and a constant shape-function for elements away from crack-tips. In this manner, the local behavior of the crack-opening-displacements (CODs) at crack-tips is correctly approximated by the square-root crack-tip shape-function. This allows us to accurately compute the dynamic stress intensity factors from the CODs. Suitable methods for evaluating the hypersingular and the strongly singular integrals are presented. Numerical examples for unbounded and bounded solids with cracks are given to show the efficiency and the accuracy of the time-domain BEM for transient elastodynamic crack analysis.

1. Introduction

Time-domain boundary element method (BEM) or time-domain boundary integral equation method (BIEM) is a promising method for transient elastodynamic crack analysis. Its semi-analytical nature, high accuracy, reduced problem dimension, and simple pre- and post-processing for input and output data are advantageous over the very developed domain-methods such as the finite element methods or the finite difference methods. Two types of BIEs are frequently used in literature, namely, the classical displacement BIEs and the traction BIEs. The classical displacement BIEs are not applicable for crack problems without domain-substructuring, since a degenerate BIE formulation arises on the mathematically degenerate crack-faces. The traction BIEs on the other hand can be applied to cracked solids without domain-substructuring, which makes the traction BIEs attractive, especially for crack analysis. Several variants of BEM formulations for crack analysis can be found in literature [2,3,6,9]: the multi-domain (domain-substructuring) method [10,11] using the classical displacement BIEs, the traction BEM [7,9,16,32–36] based on traction BIEs, the crack Green's function method [2,9] using displacement BIEs with special

☆ This paper is dedicated to Professor J.D. Achenbach, Northwestern University, USA, on the occasion of his 65th birthday.

* Tel.: +49-3583-611622; fax: +49-3583-611627.

E-mail address: c.zhang@hs-zigr.de (Ch. Zhang).

0165-2125/02/$ – see front matter
PII: S0165-2125(01)00081-6

Green's functions satisfying the traction-free boundary conditions on crack-faces, and the dual BEM [2,8,13,14] using displacement BIEs on one crack-face and traction BIEs on the other. In addition, a combined use of displacement and traction BIEs is possible, with displacement BIEs applied to external boundaries of the cracked solids and traction BIEs applied to crack-faces [22–24]. In this paper, a time-domain traction BEM is presented for two-dimensional (2D) plane strain or plane stress. Similar investigations for elastodynamic antiplane crack analysis have been presented by Gallego and Domínguez [16] and by Zhang and Savaidis [35].

Traction BIEs can be hypersingular [16,35–37], strongly singular or non-hypersingular [7,19,25,31–34], and even non-singular [21,26,28]. Hypersingular traction BIEs can be easily obtained by using Betti–Rayleigh reciprocal theorem and Hooke's law. The arising hypersingular integrals are regarded as Hadamard finite-part (HFP) integrals. A regularization of the hypersingular traction BIEs leads to strongly singular or non-hypersingular traction BIEs with Cauchy principal value (CPV) integrals. For different regularization techniques see the review articles [8,29]. Another way to immediately obtain strongly singular or non-hypersingular traction BIEs is the use of a two-state conservation integral of elastodynamics [32–34] where no regularization is required. A comparative study of hypersingular and strongly singular or non-hypersingular time-domain traction BEM was presented by Zhang and Savaidis [36,37]. The strongly singular traction BIEs can be further regularized to even non-singular traction BIEs by the so-called singularity-subtraction method [21,26,28]. The added-back terms in this method are integrated analytically.

A 2D hypersingular time-domain traction BEM is presented in this paper. Hypersingular time-domain traction BIEs are obtained by substituting the representation formula for displacement field into Hooke's law. Unlike previous BEM formulations in literature the present traction BEM is applied to both crack-faces and external boundaries of the cracked solids. A numerical solution procedure is developed for solving the hypersingular time-domain BIEs. A time-stepping scheme in conjunction with a collocation method for spatial discretization is adopted. A linear temporal shape-function is applied for temporal discretization of the crack-opening-displacements (CODs), boundary displacements and tractions. To describe the local behavior of the CODs at crack-tips, a square-root crack-tip shape-function is introduced for elements adjacent to crack-tips, while a constant shape-function used for elements is applied for elements away from crack-tips. By the way, the dynamic stress intensity factors can be computed very accurately from the numerically calculated CODs. For simplicity, the boundary displacements and tractions are approximated by constant spatial shape-functions. A direct method based on singularity-subtraction technique is used for computing the hypersingular (HFP) and the strongly singular (CPV) integrals arising in the hypersingular time-domain traction BEM. To demonstrate the accuracy and efficiency of the present method, several numerical examples for unbounded and bounded elastic solids with internal and edge cracks are presented.

2. Problem statement and hypersingular time-domain traction BIEs

We consider a homogeneous, isotropic and linearly elastic solid containing a finite crack in two-dimensional (2D) plane strain or plane stress. In the absence of body forces, the cracked solid satisfies the equations of motion [1,12]

$$\sigma_{\alpha\beta,\beta} = \rho\ddot{u}_\alpha, \tag{1}$$

the Hooke's law

$$\sigma_{\alpha\beta} = E_{\alpha\beta\gamma\delta}u_{\gamma,\delta}, \tag{2}$$

the initial conditions

$$u_\alpha(\mathbf{x}, t) = \dot{u}_\alpha(\mathbf{x}, t) = 0 \quad \text{for } t \le 0, \tag{3}$$

and the boundary conditions

$$f_\alpha(\mathbf{x}, t) = 0, \quad \mathbf{x} \in \Gamma_c, \tag{4}$$

$$f_\alpha(\mathbf{x},t) = f_\alpha^*(\mathbf{x},t), \quad \mathbf{x} \in \Gamma_\sigma, \tag{5}$$

$$u_\alpha(\mathbf{x},t) = u_\alpha^*(\mathbf{x},t), \quad \mathbf{x} \in \Gamma_u. \tag{6}$$

Here, $f_\alpha(\mathbf{x},t) = \sigma_{\alpha\beta}(\mathbf{x},t)n_\beta$ denotes the traction components, $\sigma_{\alpha\beta}$ and u_α the stress and the displacement components, ρ the mass density, $E_{\alpha\beta\gamma\delta}$ the elasticity tensor, n_β the unit normal vector, $\Gamma_c = \Gamma_c^+ + \Gamma_c^-$ with $\Gamma_c^\pm$ being the upper and the lower crack-face, Γ_σ represents the external boundary where the stresses or the tractions f_α^* are given, and Γ_u represents the external boundary where the displacements u_α^* are prescribed, respectively. A comma after a quantity designates spatial derivatives, while superscript dots stand for temporal derivatives of the quantity. The conventional summation rule over double indices is applied, with Greek indices $\alpha, \beta, \gamma = 1, 2$ for 2D plane strain or plane stress.

Generally, the initial/boundary value problem as stated above has to be solved numerically. Among many numerical methods the time-domain BEM provides an efficient way. To derive time-domain BIEs, we start with Betti–Rayleigh reciprocal theorem

$$\int_\Gamma [\sigma_{\alpha\beta}^{(1)} * u_\alpha^{(2)} - \sigma_{\alpha\beta}^{(2)} * u_\alpha^{(1)}] n_\beta \, \mathrm{d}s = 0, \tag{7}$$

where the superscript indices "(1)" and "(2)" indicate two independent elastodynamic states which satisfy the governing equations (1) and (2) as well as the initial conditions (3). In Eq. (7), an asterisk denotes Riemann convolution which is defined by

$$g(\mathbf{x},t) * h(\mathbf{x},t) = \int_0^t g(\mathbf{x}, t-\tau) h(\mathbf{x},\tau) \, \mathrm{d}\tau. \tag{8}$$

Taking Green's functions $u_{\alpha\gamma}^{\mathrm{G}}$ and $\sigma_{\alpha\beta\gamma}^{\mathrm{G}}$ for state "(1)" and the quantities u_α and $\sigma_{\alpha\beta}$ for state "(2)", a representation integral for the displacement field $u_\gamma(\mathbf{x},t)$ is obtained as

$$u_\gamma(\mathbf{x},t) = \int_\Gamma (u_{\alpha\gamma}^{\mathrm{G}} * \sigma_{\alpha\beta} - \sigma_{\alpha\beta\gamma}^{\mathrm{G}} * u_\alpha) n_\beta \, \mathrm{d}s, \quad \mathbf{x} \in \Omega, \tag{9}$$

where $u_{\alpha\gamma}^{\mathrm{G}}$ and $\sigma_{\alpha\beta\gamma}^{\mathrm{G}}$ are displacement and stress Green's functions (see Appendix A), and Ω is the interior domain of the cracked solid enclosed by its boundary $\Gamma = \Gamma_\sigma + \Gamma_u + \Gamma_c^\pm$. Applying Eq. (9) to the cracked solid and considering the continuity condition of the traction components across the crack-faces, Eq. (9) can be rewritten as

$$u_\gamma(\mathbf{x},t) = \int_{\Gamma_\sigma+\Gamma_u} (u_{\alpha\gamma}^{\mathrm{G}} * \sigma_{\alpha\beta} - \sigma_{\alpha\beta\gamma}^{\mathrm{G}} * u_\alpha) n_\beta \, \mathrm{d}s + \int_{\Gamma_c^+} \sigma_{\alpha\beta\gamma}^{\mathrm{G}} * \Delta u_\alpha n_\beta \, \mathrm{d}s, \quad \mathbf{x} \in \Omega, \tag{10}$$

with $\Delta u_\alpha(\mathbf{y},\tau)$ being the CODs defined by

$$\Delta u_\alpha(\mathbf{y},t) = u_\alpha(\mathbf{y} \in \Gamma_c^+, \tau) - u_\alpha(\mathbf{y} \in \Gamma_c^-, \tau). \tag{11}$$

As is well known that Eq. (10) cannot be directly applied to crack analysis since the usual limiting process $\mathbf{x} \to \Gamma_c^\pm$ for deriving displacement BIEs leads in this case to a degenerate BIE formulation. Several methods, such as the multi-domain (domain-substructuring) BEM, the crack Green's function BEM, the dual BEM, and the traction BEM can be applied to overcome this difficulty. In Table 1, the frequently used BEM formulations are summarized and they are illustrated in Fig. 1. A comprehensive review on advantages and drawbacks of these methods is beyond the scope of the paper, and interested readers may find detailed discussions on the subject in [3,6,34].

In this paper, we apply hypersingular time-domain traction BIEs to both crack-faces and external boundaries of the cracked solid as depicted in Fig. 1(f). An advantage of the method is that only one type of BIEs has to be

Table 1
Some variants of BEM formulations for crack analysis

Methods	Type of BIEs	
	Crack-faces	External boundaries
Multi-domain BEM	DBIE[a]	DBIE
CGF BEM[b]	No discretization	DBIE
Dual BEM	DBIE + TBIE[c]	DBIE, TBIE
DBEM[d] and TBEM[e]	TBIE	DBIE
Traction BEM	TBIE	TBIE

[a] Displacement BIEs.
[b] Crack Green's function BEM.
[c] Traction BIEs.
[d] Displacement BEM.
[e] Traction BEM.

considered instead of dealing with different kinds of BIEs. Time-domain traction BIEs can be easily obtained by substituting Eq. (10) into Hooke's law (2), letting $\mathbf{x} \to \Gamma_\sigma + \Gamma_u + \Gamma_c^+$ and invoking the boundary conditions (4)–(6). This results in

$$\delta(\mathbf{x}) f_\alpha(\mathbf{x}, t) = n_\beta(\mathbf{x}) \int_{\Gamma_\sigma + \Gamma_u} (U^{\mathrm{G}}_{\gamma\alpha\beta} * f_\gamma - T^{\mathrm{G}}_{\gamma\alpha\beta} * u_\gamma)\, \mathrm{d}s + n_\beta(\mathbf{x}) \int_{\Gamma_c^+} T^{\mathrm{G}}_{\gamma\alpha\beta} * \Delta u_\gamma \, \mathrm{d}s, \quad \mathbf{x} \in \Gamma, \tag{12}$$

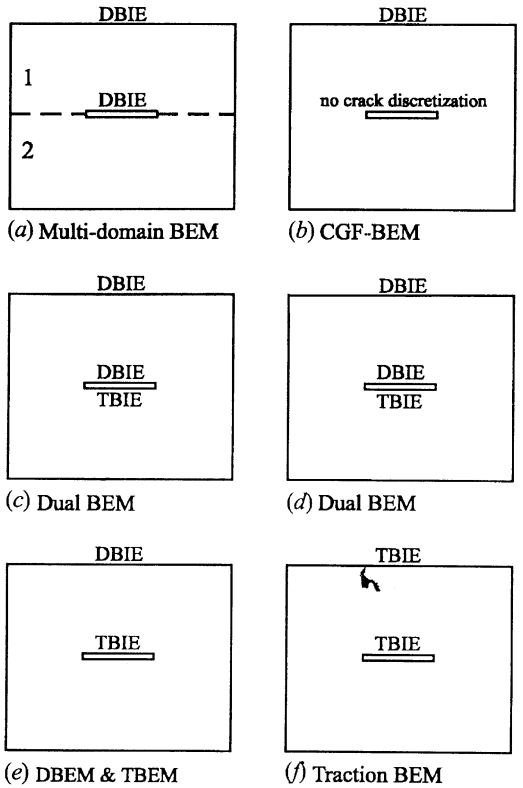

Fig. 1. Some variants of BEM for crack analysis.

where

$$\delta(\mathbf{x}) = \begin{cases} \frac{1}{2}, & \mathbf{x} \in \Gamma_\sigma + \Gamma_u, \\ 1, & \mathbf{x} \in \Gamma_c, \end{cases} \tag{13}$$

and

$$U^G_{\gamma\alpha\beta} = -E_{\alpha\beta\delta\lambda} u^G_{\delta\gamma,\lambda} = -\sigma^G_{\alpha\beta\gamma}, \qquad T^G_{\gamma\alpha\beta} = -E_{\alpha\beta\delta\lambda}\sigma^G_{\gamma\eta\delta,\lambda} n_\eta. \tag{14}$$

In Eq. (13), smooth external boundaries Γ_σ and Γ_u are assumed. Green's functions $U^G_{\gamma\alpha\beta}$ and $T^G_{\gamma\alpha\beta}$ are given in Appendix A. The traction BIEs (12) are hypersingular since in 2D case $T^G_{\gamma\alpha\beta}$ behaves as

$$T^G_{\gamma\alpha\beta}(\mathbf{x}, t; \mathbf{y}, \tau) \propto \frac{1}{|\mathbf{x} - \mathbf{y}|^2} \quad \text{for } \mathbf{x} \to \mathbf{y}. \tag{15}$$

Here, the hypersingular integrals are regarded as Hadamard "finite-part" integrals. The hypersingular traction BIEs (12) can be solved numerically by different ways such as the Galerkin method [4,5], the regularization method [7,27,29] and the direct method [16,35–37]. The Galerkin method is self-regularizing through repeated temporal/spatial integrations. The regularization method first reduces hypersingular integrals to strongly singular CPV integrals and then solves the regularized BIEs numerically by the commonly applied numerical methods for displacement BIEs. In the direct method, the hypersingular integrals are directly evaluated analytically and numerically by suitable techniques. In this paper, a direct method is applied for solving the hypersingular time-domain traction BIEs numerically.

3. Numerical solution procedure

3.1. Discretization of the time-domain traction BIEs

In this section, a time-stepping scheme is presented for solving the hypersingular time-domain traction BIEs numerically. The crack-face, the external boundaries of the cracked solid, and the time variable t are discretized as follows:

$$\Gamma = \sum_{e=1}^{E} \Gamma_e, \qquad t = \sum_{n=1}^{N} n\Delta t, \tag{16}$$

where $\Gamma = \Gamma_\sigma + \Gamma_u + \Gamma_c^+$ with Γ_e denoting the eth element, $E = E_1 + E_2$ is the total element-number with E_1 being the element-number for the crack-face and E_2 being the element-number for the external boundaries, and Δt represents a constant time-step, respectively. The unknown CODs and other boundary quantities are approximated by the following interpolation functions:

$$\Delta u_\gamma(\mathbf{y}, \tau) = \sum_{e=1}^{E_1}\sum_{n=1}^{N} \mu_{e(\Delta u)}(\mathbf{y})\eta^n_{(\Delta u)}(\tau)(\Delta u_\gamma)^n_e, \tag{17}$$

$$u_\gamma(\mathbf{y}, \tau) = \sum_{e=1}^{E_2}\sum_{n=1}^{N} \mu_{e(u)}(\mathbf{y})\eta^n_{(u)}(\tau)(u_\gamma)^n_e, \tag{18}$$

$$f_\gamma(\mathbf{y}, \tau) = \sum_{e=1}^{E_2}\sum_{n=1}^{N} \mu_{e(f)}(\mathbf{y})\eta^n_{(f)}(\tau)(f_\gamma)^n_e, \tag{19}$$

where $\mu_{e(\cdot)}(\mathbf{y})$ and $\eta^n_{(\cdot)}(\tau)$ are the spatial and the temporal shape-functions. The spatial shape-function can be expressed as

$$\mu_{e(\cdot)}(\mathbf{y}) = g_{(\cdot)}(\mathbf{y})H(\mathbf{y}) = \begin{cases} g_{(\cdot)}(\mathbf{y}), & \mathbf{y} \in \Gamma_e, \\ 0, & \mathbf{y} \notin \Gamma_e, \end{cases} \tag{20}$$

in which the function $g_{(\cdot)}(\mathbf{y})$ describes the spatial variation of the unknown quantities within the eth element and $H(\mathbf{y})$ is the Heaviside function. The temporal variation of the CODs and the boundary displacements is approximated by a linear shape-function as

$$\eta^n_{(\Delta u)}(\tau) = \eta^n_{(u)}(\tau) = \begin{cases} 1 - \dfrac{|\tau - n\Delta t|}{\Delta t}, & |\tau - n\Delta t| \le \Delta t, \\ 0, & \text{otherwise.} \end{cases} \tag{21}$$

For the temporal discretization of the boundary tractions, either a linear temporal shape-function

$$\eta^n_{(f)}(\tau) = \begin{cases} 1 - \dfrac{|\tau - n\Delta t|}{\Delta t}, & |\tau - n\Delta t| \le \Delta t, \\ 0, & \text{otherwise,} \end{cases} \tag{22}$$

or a constant temporal shape-function

$$\eta^n_{(f)}(\tau) = \begin{cases} 1, & (n-1)\Delta t \le \tau \le n\Delta t, \\ 0, & \text{otherwise} \end{cases} \tag{23}$$

is used for the purpose of comparison.

Substitution of Eqs. (17)–(19) into the hypersingular BIEs (12) results in a system of linear algebraic equations

$$\sum_{n=1}^{N} \left[\sum_{e=1}^{E_1} A^{mn}_{\gamma\alpha;ed} (\Delta u_\gamma)^n_e + \sum_{e=1}^{E_2} B^{mn}_{\gamma\alpha;ed} (u_\gamma)^n_e + \sum_{e=1}^{E_2} C^{mn}_{\gamma\alpha;ed} (f_\gamma)^n_e \right] = \delta_d (f_\alpha)^m_d, \tag{24}$$

where $\delta_d = \delta(\mathbf{x}_d)$ and the system matrices $A^{mn}_{\gamma\alpha;ed}$, $B^{mn}_{\gamma\alpha;ed}$ and $C^{mn}_{\gamma\alpha;ed}$ are given by

$$A^{mn}_{\gamma\alpha;ed} = n_\beta(\mathbf{x}_d) \int_{t_{n-1}}^{t_{n+1}} \left[\int_{\Gamma_e} T^{\mathrm{G}}_{\gamma\alpha\beta}(\mathbf{x}_d, t_m; \mathbf{y}, \tau) \mu_{e(\Delta u)}(\mathbf{y}) \, \mathrm{d}s \right] \eta^n_{(\Delta u)}(\tau) \, \mathrm{d}\tau, \tag{25}$$

$$B^{mn}_{\gamma\alpha;ed} = -n_\beta(\mathbf{x}_d) \int_{t_{n-1}}^{t_{n+1}} \left[\int_{\Gamma_e} T^{\mathrm{G}}_{\gamma\alpha\beta}(\mathbf{x}_d, t_m; \mathbf{y}, \tau) \mu_{e(u)}(\mathbf{y}) \, \mathrm{d}s \right] \eta^n_{(u)}(\tau) \, \mathrm{d}\tau, \tag{26}$$

$$C^{mn}_{\gamma\alpha;ed} = n_\beta(\mathbf{x}_d) \int_{t_{n-1}}^{t_{n+1}} \left[\int_{\Gamma_e} U^{\mathrm{G}}_{\gamma\alpha\beta}(\mathbf{x}_d, t_m; \mathbf{y}, \tau) \mu_{e(f)}(\mathbf{y}) \, \mathrm{d}s \right] \eta^n_{(f)}(\tau) \, \mathrm{d}\tau. \tag{27}$$

3.2. Computation of the system matrices

With the linear temporal shape-function (21) or (22), time-integrations arising in the system matrices $A^{mn}_{\gamma\alpha;ed}$, $B^{mn}_{\gamma\alpha;ed}$ and $C^{mn}_{\gamma\alpha;ed}$ can be carried out analytically. After analytical time-integrations, the system matrices take the following forms:

$$A^{mn}_{\gamma\alpha;ed} = n_\beta(\mathbf{x}_d) \int_{\Gamma_e} T^{*}_{\gamma\alpha\beta}(\mathbf{x}_d, t_m; \mathbf{y}, t_n) \mu_{e(\Delta u)}(\mathbf{y}) \, \mathrm{d}s, \tag{28}$$

$$B^{mn}_{\gamma\alpha;ed} = -n_\beta(\mathbf{x}_d) \int_{\Gamma_e} T^{*}_{\gamma\alpha\beta}(\mathbf{x}_d, t_m; \mathbf{y}, t_n) \mu_{e(u)}(\mathbf{y}) \, \mathrm{d}s, \tag{29}$$

$$C^{mn}_{\gamma\alpha;ed} = n_\beta(\mathbf{x}_d)\int_{\Gamma_e} U^*_{\gamma\alpha\beta}(\mathbf{x}_d, t_m; \mathbf{y}, t_n)\mu_{e(f)}(\mathbf{y})\,\mathrm{d}s, \tag{30}$$

where the functions $T^*_{\gamma\alpha\beta}$ and $U^*_{\gamma\alpha\beta}$ are given by

$$\begin{aligned} T^*_{\gamma\alpha\beta} &= \int_{(n-1)\Delta t}^{(n+1)\Delta t} T^{\mathrm{G}}_{\gamma\alpha\beta}(\mathbf{x}_d, t_m; \mathbf{y}, \tau)\eta^n_{(u)}(\tau)\,\mathrm{d}\tau \\ &= \frac{\mu}{(2\pi c_{\mathrm{T}}\Delta t)r^2}\left[-\frac{2}{\kappa^3}(D^{\mathrm{L}}_{\gamma\alpha\beta} + E^{\mathrm{L}}_{\gamma\alpha\beta})P_{\mathrm{L}} + 2(D^{\mathrm{T}}_{\gamma\alpha\beta} + E^{\mathrm{T}}_{\gamma\alpha\beta})P_{\mathrm{T}} + \left(\frac{4}{3r^2}\right)C_{\gamma\alpha\beta}\left(\frac{1}{\kappa^3}Q_{\mathrm{L}} - Q_{\mathrm{T}}\right)\right. \\ &\quad \left. -r^2\left(\frac{1}{\kappa^3}D^{\mathrm{L}}_{\gamma\alpha\beta}S_{\mathrm{L}} - D^{\mathrm{T}}_{\gamma\alpha\beta}S_{\mathrm{T}}\right)\right], \end{aligned} \tag{31}$$

$$\begin{aligned} U^*_{\gamma\alpha\beta} &= \int_{(n-1)\Delta t}^{(n+1)\Delta t} U^{\mathrm{G}}_{\gamma\alpha\beta}(\mathbf{x}_d, t_m; \mathbf{y}, \tau)\eta^n_{(f)}(\tau)\,\mathrm{d}\tau \\ &= \frac{1}{(2\pi c_{\mathrm{T}}\Delta t)r}\left[\frac{1}{\kappa^3}B^{\mathrm{L}}_{\alpha\beta\gamma}P_{\mathrm{L}} - B^{\mathrm{T}}_{\alpha\beta\gamma}P_{\mathrm{T}} - \left(\frac{1}{3r^2}\right)A_{\alpha\beta\gamma}\left(\frac{1}{\kappa^3}Q_{\mathrm{L}} - Q_{\mathrm{T}}\right)\right], \end{aligned} \tag{32}$$

in which $r = |\mathbf{x}_d - \mathbf{y}|$, and $\kappa = c_{\mathrm{L}}/c_{\mathrm{T}}$ with c_{L} and c_{T} being the longitudinal and the transverse wave velocity.

$$c_{\mathrm{L}} = \sqrt{\frac{\lambda + 2\mu}{\rho}}, \qquad c_{\mathrm{T}} = \sqrt{\frac{\mu}{\rho}}, \tag{33}$$

where λ and μ are Lamé's elastic constants. The auxiliary functions in Eqs. (31) and (32) are given by

$$P_\xi = \sum_{q=-1}^{+1}(-2)^{1-|q|}H[(m-n+q)c_\xi\Delta t - r]\sqrt{(m-n+q)^2(c_\xi\Delta t)^2 - r^2}, \tag{34}$$

$$Q_\xi = \sum_{q=-1}^{+1}(-2)^{1-|q|}H[(m-n+q)c_\xi\Delta t - r]\sqrt{[(m-n+q)^2(c_\xi\Delta t)^2 - r^2]^3}, \tag{35}$$

$$S_\xi = \sum_{q=-1}^{+1}(-2)^{1-|q|}\frac{H[(m-n+q)c_\xi\Delta t - r]}{\sqrt{(m-n+q)^2(c_\xi\Delta t)^2 - r^2}}. \tag{36}$$

where $\xi = \mathrm{L}, \mathrm{T}$. The auxiliary functions $A_{\alpha\beta\gamma}$, $B^\xi_{\alpha\beta\gamma}$, $C_{\gamma\alpha\beta}$, $D^\xi_{\gamma\alpha\beta}$ and $E^\xi_{\gamma\alpha\beta}$ are given in Appendix A.

When a constant temporal shape-function Eq. (23) is used for the boundary tractions, the time-integrations arising in the system matrix $C_{\gamma\alpha\beta}$ can also be performed analytically. The corresponding result is obtained as

$$\begin{aligned} U^*_{\gamma\alpha\beta} &= \int_{(n-1)\Delta t}^{n\Delta t} U^{\mathrm{G}}_{\gamma\alpha\beta}(\mathbf{x}, t_m; \mathbf{y}, \tau)\eta^n_{(f)}(\tau)\,\mathrm{d}\tau \\ &= \frac{1}{2\pi r}\left[\frac{1}{\kappa^2}B^{\mathrm{L}}_{\alpha\beta\gamma}V_{\mathrm{L}} - B^{\mathrm{T}}_{\alpha\beta\gamma}V_{\mathrm{T}} - \left(\frac{1}{r^2}\right)A_{\alpha\beta\gamma}\left(\frac{1}{\kappa^2}W_{\mathrm{L}} - W_{\mathrm{T}}\right)\right], \end{aligned} \tag{37}$$

where

$$V_\xi = \sum_{q=0}^{+1}(-1)^{1-q}H[(m-n+q)c_\xi\Delta t - r]\frac{(m-n+q)c_\xi\Delta t}{\sqrt{(m-n+q)^2(c_\xi\Delta t)^2 - r^2}}, \tag{38}$$

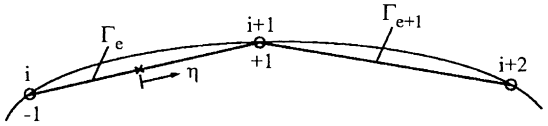

Fig. 2. Local coordinate system.

$$W_\xi = \sum_{q=0}^{+1}(-1)^{1-q} H[(m-n+q)c_\xi \Delta t - r](m-n+q)c_\xi \Delta t \times \sqrt{(m-n+q)^2(c_\xi \Delta t)^2 - r^2}. \tag{39}$$

In the case of $\mathbf{x}_d \notin \Gamma_e$, spatial integrations arising in the system matrices (28)–(30) can be carried out numerically by using standard Gaussian quadrature, since all integrals are regular. For $\mathbf{x}_d \in \Gamma_e$, however, hypersingularities may occur in Eqs. (28) and (29), while strong singularities may arise in Eq. (30). Thus, special attention should be paid to this case.

For the evaluation of the integrals arising in the system matrices $A^{mn}_{\gamma\alpha;ed}$, $B^{mn}_{\gamma\alpha;ed}$ and $C^{mn}_{\gamma\alpha;ed}$ when $\mathbf{x}_d \in \Gamma_e$, it is convenient to introduce a local coordinate system $\eta \in [-1, +1]$ with its origin at the midpoint of the eth element Γ_e. For straight-elements used in the present method the following relations are valid:

$$\begin{aligned} &\mathrm{d}s = J\,\mathrm{d}\eta, \qquad r_{,\alpha}n_\alpha = 0, \qquad r_\alpha r_\beta = R_{\alpha\beta}(\eta-\eta^*)^2, \qquad r^2 = J^2(\eta-\eta^*)^2, \qquad r_{,\alpha}r_{,\beta} = \frac{R_{\alpha\beta}}{J^2}, \\ &R_{\alpha\beta} = \tfrac{1}{4}(y^{i+1}_\alpha - y^i_\alpha)(y^{i+1}_\beta - y^i_\beta), \qquad J = \sqrt{R_{\alpha\alpha}}, \end{aligned} \tag{40}$$

where the superscripts "i" and "$i+1$" designate the ith and the $(i+1)$th node of the eth element, see Fig. 2.

Let us first consider the system matrix $A^{mn}_{\gamma\alpha;ed}$. With the relations of Eq. (40) and using the abbreviation

$$g(\eta) = \mu_{e(\Delta u)}(\eta), \tag{41}$$

the system matrix $A^{mn}_{\gamma\alpha;ed}$ as given by Eq. (28) can be recast into the form

$$\begin{aligned} A^{mn}_{\gamma\alpha;ed} &= n_\beta(\mathbf{x}_d)\int_{\Gamma_e} T^*_{\gamma\alpha\beta}(\mathbf{x}, t_m; \mathbf{y}, t_n)\mu_{e(\Delta u)}(\mathbf{y})\,\mathrm{d}s \\ &= \frac{\mu}{2\pi c_\mathrm{T}\Delta t J}\left\{ 2\sum_{\xi=\mathrm{L,T}} a_\xi (D^\xi_{\gamma\alpha\beta} + E^\xi_{\gamma\alpha\beta})n_\beta \int_{-1}^{+1} \frac{1}{(\eta-\eta^*)^2} P_\xi(\eta,\eta^*)g(\eta)\,\mathrm{d}\eta \right. \\ &\qquad - \left(\frac{4}{3}\right) C_{\gamma\alpha\beta}n_\beta \int_{-1}^{+1} \frac{1}{(\eta-\eta^*)^2} \sum_{\xi=\mathrm{L,T}} \frac{1}{J^2(\eta-\eta^*)^2} a_\xi Q_\xi(\eta,\eta^*)g(\eta)\,\mathrm{d}\eta \\ &\qquad \left. + J^2 \sum_{\xi=\mathrm{L,T}} a_\xi D^\xi_{\gamma\alpha\beta}n_\beta \int_{-1}^{+1} S_\xi(\eta,\eta^*)g(\eta)\,\mathrm{d}\eta \right\}, \end{aligned} \tag{42}$$

where

$$a_\xi = \begin{cases} -\kappa^{-3}, & \xi = \mathrm{L}, \\ 1, & \xi = \mathrm{T}. \end{cases} \tag{43}$$

It should be noted here that the functions $D^\xi_{\gamma\alpha\beta}n_\beta$, $E^\xi_{\gamma\alpha\beta}n_\beta$ and $C_{\gamma\alpha\beta}n_\beta$ appearing in Eq. (42) are independent of the integration variable η, see Appendix B. To proceed the discussion, two different situations should be distinguished

now, namely, $m \neq n$ and $m = n$. For $m \neq n$, all integrals in the system matrix $A^{mn}_{\gamma\alpha;ed}$ are regular at $\eta = \eta^*$, since

$$P_\xi \propto (\eta - \eta^*)^2, \quad \eta \to \eta^*, \tag{44}$$

$$\sum_{\xi=\mathrm{L,T}} \frac{1}{J^2(\eta-\eta^*)^2} a_\xi Q_\xi \propto -(\eta-\eta^*)^2, \quad \eta \to \eta^*. \tag{45}$$

Consequently, all integrals appearing in Eq. (42) can be integrated numerically by using standard Gaussian quadrature. For $m = n$, however, the first two integrals of Eq. (42) are hypersingular while the last integral is still regular at $\eta = \eta^*$ because

$$P_\xi \propto c_\xi \Delta t, \quad \eta \to \eta^*, \tag{46}$$

$$\sum_{\xi=\mathrm{L,T}} \frac{1}{J^2(\eta-\eta^*)^2} a_\xi Q_\xi \propto \alpha_1 c_\mathrm{T} \Delta t, \quad \eta \to \eta^*, \tag{47}$$

in which

$$\alpha_1 = \tfrac{3}{2}(1 - \kappa^{-2}). \tag{48}$$

Different techniques are available for computing hypersingular and strongly singular integrals. Recent advances and applications of these techniques to BEM can be found in [27]. Here, a semi-analytical method, the so-called singularity-subtraction method is applied. The key steps of the method are summarized in Appendix C. By using this technique, the first two integrals in Eq. (42) can be rewritten as

$$\begin{aligned}
&\int_{-1}^{+1} \frac{1}{(\eta-\eta^*)^2} P_\xi(\eta,\eta^*) g(\eta)\,\mathrm{d}\eta \\
&\quad = \int_{-1}^{+1} \frac{1}{(\eta-\eta^*)^2} \left[P_\xi(\eta,\eta^*) g(\eta) - c_\xi \Delta t g(\eta^*) - c_\xi \Delta t (\eta-\eta^*) \left.\frac{\partial g}{\partial \eta}\right|_{\eta=\eta^*} \right] \mathrm{d}\eta \\
&\qquad - \frac{2c_\xi \Delta t}{1-\eta^{*2}} g(\eta^*) + c_\xi \Delta t \ln\left|\frac{1-\eta^*}{1+\eta^*}\right| \left.\frac{\partial g}{\partial \eta}\right|_{\eta=\eta^*},
\end{aligned} \tag{49}$$

$$\begin{aligned}
&\int_{-1}^{+1} \frac{1}{(\eta-\eta^*)^2} \sum_{\xi=\mathrm{L,T}} \frac{1}{J^2(\eta-\eta^*)^2} a_\xi Q_\xi(\eta,\eta^*) g(\eta)\,\mathrm{d}\eta \\
&\quad = \int_{-1}^{+1} \frac{1}{(\eta-\eta^*)^2} \left[h_1(\eta,\eta^*) g(\eta) - \alpha_1 c_\mathrm{T} \Delta t\, g(\eta^*) - \alpha_1 c_\mathrm{T} \Delta t (\eta-\eta^*) \left.\frac{\partial g}{\partial \eta}\right|_{\eta=\eta^*} \right] \mathrm{d}\eta \\
&\qquad - \frac{2\alpha_1 c_\mathrm{T} \Delta t}{1-\eta^{*2}} g(\eta^*) + \alpha_1 c_\mathrm{T} \Delta t \ln\left|\frac{1-\eta^*}{1+\eta^*}\right| \left.\frac{\partial g}{\partial \eta}\right|_{\eta=\eta^*},
\end{aligned} \tag{50}$$

where

$$h_1(\eta,\eta^*) = \sum_{\xi=\mathrm{L,T}} \frac{1}{J^2(\eta-\eta^*)^2} a_\xi Q_\xi(\eta,\eta^*), \tag{51}$$

and the following relations are used:

$$P_\xi(\eta,\eta^*)|_{\eta=\eta^*} = c_\xi \Delta t, \quad \left.\frac{\partial P_\xi}{\partial \eta}\right|_{\eta=\eta^*} = 0, \tag{52}$$

$$h_1(\eta,\eta^*)|_{\eta=\eta^*}=\alpha_1 c_T\Delta t,\qquad \left.\frac{\partial h_1}{\partial\eta}\right|_{\eta=\eta^*}=0. \tag{53}$$

The integrals in Eqs. (49) and (50) are regular and they can be integrated numerically by standard Gaussian quadrature.

The semi-analytical procedure for spatial integration presented here requires that the CODs and their derivatives should satisfy Hölder continuity condition, i.e. the CODs must be $C^{1,\alpha}$ continuous. This continuity requirement is in the present method ensured, since the collocation points are selected as the element midpoints and do not coincide with the crack-tips where the CODs are no longer $C^{1,\alpha}$ continuous. If higher order such as linear or quadratic spatial shape-functions are used, the $C^{1,\alpha}$-continuity requirement of the CODs is satisfied only when the collocation points do not coincide with the element-nodes at crack-tips. This is the case if discontinuous elements with collocation points located at interior element-nodes are applied [2,13,14]. Another way to ensure the $C^{1,\alpha}$-continuity condition was presented by Gallego and Domínguez [16], who used continuous quadratic elements with collocation points positioned at interior element-points instead of element-nodes.

The matrix $B^{mn}_{\gamma\alpha;ed}$ as given by Eq. (29) has the same structure $A^{mn}_{\gamma\alpha;ed}$ and it can be treated by the same way, but the procedure will not be repeated here.

Now we continue to consider the system matrix $C^{mn}_{\gamma\alpha;ed}$ given by Eq. (30). Using the relations of Eq. (40) and the abbreviation

$$h(\eta)=\mu_{e(f)}(\eta), \tag{54}$$

the system matrix $C^{mn}_{\gamma\alpha;ed}$ is rewritten as

$$\begin{aligned}C^{mn}_{\gamma\alpha;ed}&=n_\beta(\mathbf{x}_d)\int_{\Gamma_e}U^*_{\gamma\alpha\beta}(\mathbf{x}_d,t_m;\mathbf{y},t_n)\mu_{e(f)}(\mathbf{y})\,\mathrm{d}s\\&=\frac{1}{2\pi c_T\Delta t\,J}\left\{\sum_{\xi=\mathrm{L,T}}a_\xi B^\xi_{\alpha\beta\gamma}n_\beta\int_{-1}^{+1}\frac{1}{\eta-\eta^*}P_\xi(\eta,\eta^*)h(\eta)\,\mathrm{d}\eta\right.\\&\qquad\left.+\frac{1}{3}A_{\alpha\beta\gamma}n_\beta\int_{-1}^{+1}\frac{1}{\eta-\eta^*}\sum_{\xi=\mathrm{L,T}}\frac{1}{J^2(\eta-\eta^*)^2}a_\xi Q_\xi(\eta,\eta^*)h(\eta)\,\mathrm{d}\eta\right\}.\end{aligned} \tag{55}$$

For $m\neq n$, the integrals in Eq. (55) are again regular and they can be evaluated numerically by using standard Gaussian quadrature. For $m=n$, the integrals are CPV integrals which can be evaluated analytically and numerically by using the singularity-subtraction technique as given in Appendix C. The method yields finally the following results:

$$\int_{-1}^{+1}\frac{1}{\eta-\eta^*}P_\xi(\eta,\eta^*)h(\eta)\,\mathrm{d}\eta=\int_{-1}^{+1}\frac{1}{\eta-\eta^*}[P_\xi(\eta,\eta^*)h(\eta)-c_\xi\Delta t\,h(\eta^*)]\,\mathrm{d}\eta+c_\xi\Delta t\ln\left|\frac{1-\eta^*}{1+\eta^*}\right|h(\eta^*), \tag{56}$$

$$\begin{aligned}&\int_{-1}^{+1}\frac{1}{\eta-\eta^*}\sum_{\xi=\mathrm{L,T}}\frac{1}{J^2(\eta-\eta^*)^2}a_\xi Q_\xi(\eta,\eta^*)h(\eta)\,\mathrm{d}\eta\\&\quad=\int_{-1}^{+1}\frac{1}{\eta-\eta^*}[h_1(\eta,\eta^*)h(\eta)-\alpha_1c_T\Delta t\,h(\eta^*)]\,\mathrm{d}\eta+\alpha_1c_T\Delta t\ln\left|\frac{1-\eta^*}{1+\eta^*}\right|h(\eta^*),\end{aligned} \tag{57}$$

where use is made of Eqs. (46), (47) and (51)–(53). Here again, the integrals in Eqs. (56) and (57) are regular and they provide no numerical difficulties by using standard Gaussian quadrature.

For comparison purpose, a constant temporal shape-function for boundary tractions, see Eq. (23), is also used in the present investigation. In this case, the system matrix $C^{mn}_{\gamma\alpha;ed}$ takes the following form:

$$C^{mn}_{\gamma\alpha;ed} = n_\beta(\mathbf{x}_d)\int_{\Gamma_e} U^*_{\gamma\alpha\beta}(\mathbf{x}_d, t_m; \mathbf{y}, t_n)\mu_{e(f)}(\mathbf{y})\,\mathrm{d}s$$
$$= \frac{1}{2\pi}\left\{ -\sum_{\xi=\mathrm{L,T}} b_\xi B^\xi_{\alpha\beta\gamma} n_\beta \int_{-1}^{+1} \frac{1}{\eta-\eta^*} V_\xi(\eta,\eta^*)h(\eta)\,\mathrm{d}\eta \right.$$
$$\left. + A_{\alpha\beta\gamma} n_\beta \int_{-1}^{+1} \frac{1}{\eta-\eta^*} \sum_{\xi=\mathrm{L,T}} \frac{1}{J^2(\eta-\eta^*)^2} b_\xi W_\xi(\eta,\eta^*)h(\eta)\,\mathrm{d}\eta \right\}, \tag{58}$$

where

$$b_\xi = \begin{cases} -\kappa^{-2}, & \xi = \mathrm{L}, \\ 1, & \xi = \mathrm{T}. \end{cases} \tag{59}$$

By appealing to the following asymptotics for $m \neq n$ and $\eta \to \eta^*$

$$V_\xi \propto (\eta-\eta^*)^2, \quad \eta \to \eta^*, \tag{60}$$

$$\sum_{\xi=\mathrm{L,T}} \frac{1}{J^2(\eta-\eta^*)^2} b_\xi W_\xi \propto (\eta-\eta^*)^2, \quad \eta \to \eta^*, \tag{61}$$

it can be easily seen that the integrals of Eq. (58) are regular and they can be integrated numerically by standard Gaussian quadrature. For $m = n$, however, the integrals of Eq. (58) are CPV integrals since

$$V_\xi \propto 1, \quad \eta \to \eta^*, \tag{62}$$

$$\sum_{\xi=\mathrm{L,T}} \frac{1}{J^2(\eta-\eta^*)^2} b_\xi W_\xi \propto \frac{1}{2}(\kappa^{-2}-1), \quad \eta \to \eta^*. \tag{63}$$

Application of the singularity-subtraction technique to the CPV integrals of Eq. (58) yields

$$\int_{-1}^{+1} \frac{1}{\eta-\eta^*} V_\xi(\eta,\eta^*)h(\eta)\,\mathrm{d}\eta = \int_{-1}^{+1} \frac{1}{\eta-\eta^*}[V_\xi(\eta,\eta^*)h(\eta) - h(\eta^*)]\,\mathrm{d}\eta + \ln\left|\frac{1-\eta^*}{1+\eta^*}\right| h(\eta^*), \tag{64}$$

$$\int_{-1}^{+1} \frac{1}{\eta-\eta^*} \sum_{\xi=\mathrm{L,T}} \frac{1}{J^2(\eta-\eta^*)^2} b_\xi Q_\xi(\eta,\eta^*)h(\eta)\,\mathrm{d}\eta$$
$$= \int_{-1}^{+1} \frac{1}{\eta-\eta^*}[h_2(\eta,\eta^*)h(\eta) - \alpha_2 h(\eta^*)]\,\mathrm{d}\eta + \alpha_2 \ln\left|\frac{1-\eta^*}{1+\eta^*}\right| h(\eta^*), \tag{65}$$

where

$$h_2(\eta,\eta^*) = \sum_{\xi=\mathrm{L,T}} \frac{1}{J^2(\eta-\eta^*)^2} b_\xi W_\xi(\eta,\eta^*), \qquad \alpha_2 = \tfrac{1}{2}(\kappa^{-2}-1), \tag{66}$$

and use is made of the following relations:

$$V_\xi(\eta,\eta^*)|_{\eta=\eta^*} = 1, \qquad h_2(\eta,\eta^*)|_{\eta=\eta^*} = \alpha_2. \tag{67}$$

The integrals in Eqs. (64) and (65) are again regular and can thus be integrated numerically by standard Gaussian quadrature.

Table 2
Adopted temporal and spatial shape-functions

Boundary data	Temporal	Spatial
CODs	Linear	CTE[a] at crack-tips, constant otherwise
Displacements	Linear	Constant
Tractions	Linear, constant	Constant

[a] Crack-tip element.

Two different spatial shape-functions are adopted for approximating the spatial variation of the CODs. For simplicity, a constant spatial shape-function is applied for elements away from crack-tips, while a square-root crack-tip shape-function is used for elements adjacent to crack-tips. In this manner, the local behavior of the CODs at crack-tips is properly described. In addition, crack-tip element is also used as a "transition element" for the second element behind the crack-tips. The use of the so-called "transition elements" improves the accuracy of the computed dynamic stress intensity factors. On external boundaries of the cracked solid, both the displacements and the tractions are approximated by constant spatial shape-functions for simplicity. Table 2 summarizes the adopted temporal and spatial shape-functions in the present investigation.

It should be noted here that the spatial integration of singular integrals, i.e., diagonal terms, of the system matrices $A^{mn}_{\gamma\alpha;ed}$, $B^{mn}_{\gamma\alpha;ed}$ and $C^{mn}_{\gamma\alpha;ed}$ can be performed analytically when a constant spatial shape-function $\mu_{e(\Delta u)} = \mu_{e(u)} = \mu_{e(f)} = 1$ is used. Note also that the integrands have a integrable singularity at the wave fronts $c_{\mathrm{L}}(t-\tau) = r$ and $c_{\mathrm{T}}(t-\tau) = r$ which provides no difficulties by using standard Gaussian quadrature. The methods used for temporal and spatial integrations in computing the system matrices are summarized in Table 3.

3.3. Time-stepping scheme

By using the causality property and the time-translation invariance of Green's functions (see Appendix A), it can be easily shown that the system matrix $A^{mn}_{\gamma\alpha;ed}$ has the following special form:

$$\begin{bmatrix} \mathbf{A}^{11} & & & \\ \mathbf{A}^{21} & \mathbf{A}^{22} & & 0 \\ \mathbf{A}^{31} & \mathbf{A}^{32} & \mathbf{A}^{33} & \\ \cdot & \cdot & \cdot & \\ \mathbf{A}^{m1} & \mathbf{A}^{m2} & \cdots & \mathbf{A}^{mm} \end{bmatrix} = \begin{bmatrix} \mathbf{A}^{1} & & & \\ \mathbf{A}^{2} & \mathbf{A}^{1} & & 0 \\ \mathbf{A}^{3} & \mathbf{A}^{2} & \mathbf{A}^{1} & \\ \cdot & \cdot & \cdot & \\ \mathbf{A}^{q} & \mathbf{A}^{q-1} & \cdots & \mathbf{A}^{1} \end{bmatrix}, \tag{68}$$

Table 3
Methods used for temporal and spatial integrations

Matrices	Temporal integration	Spatial integration			
		$\mathbf{x}_d \notin \Gamma_e$		$\mathbf{x}_d \in \Gamma_e$	
		Integrals	Integration	Integrals	Integration
$A^{mn}_{\gamma\alpha;ed}$	Analytically	Regular	Gaussian[a]	$m \neq n$: regular, $m = n$: HFP[b]	Gaussian, SSTM[c]
$B^{mn}_{\gamma\alpha;ed}$	Analytically	Regular	Gaussian	$m \neq n$: regular, $m = n$: HFP	Gaussian, SSTM
$C^{mn}_{\gamma\alpha;ed}$	Analytically	Regular	Gaussian	$m \neq n$: regular, $m = n$: CPV[d]	Gaussian, SSTM

[a] Gaussian quadrature.
[b] Hardamard finite-part integrals.
[c] Singularity-subtraction method.
[d] Cauchy principal value integrals.

where $q = m - n + 1$. Obviously, the matrices $B^{mn}_{\gamma\alpha;ed}$ and $C^{mn}_{\gamma\alpha;ed}$ obey the same structure as $A^{mn}_{\gamma\alpha;ed}$ does.

For convenience, the system of linear algebraic equations (24) is rewritten in matrix form as

$$\bar{\mathbf{A}}^1\mathbf{v}^q = \bar{\mathbf{C}}^1\mathbf{f}^q + \sum_{s=1}^{q-1}(\bar{\mathbf{C}}^{q-s+1}\mathbf{f}^s - \bar{\mathbf{A}}^{q-s+1}\mathbf{v}^s), \tag{69}$$

where the matrix $\bar{\mathbf{A}}^s$ consists of the matrices $\mathbf{A}^s$ and $\mathbf{B}^s$, the matrix $\bar{\mathbf{C}}^s$ consists of the matrix $\mathbf{C}^s$ and the unit matrix $\mathbf{I}$, $\mathbf{v}^s$ is a vector containing the CODs on crack-faces and the displacements on external boundaries of the cracked solid, and $\mathbf{f}^s$ is the traction vector on discrete boundary points, respectively. By invoking the boundary conditions (4)–(6), Eq. (69) can be recast into the following form:

$$\bar{\mathbf{B}}^1\mathbf{x}^q = \bar{\mathbf{D}}^1\mathbf{y}^q + \sum_{s=1}^{q-1}(\bar{\mathbf{C}}^{q-s+1}\mathbf{f}^s - \bar{\mathbf{A}}^{q-s+1}\mathbf{v}^s), \tag{70}$$

in which $\bar{\mathbf{B}}^1$ and $\bar{\mathbf{D}}^1$ are the reordered system matrices from $\bar{\mathbf{A}}^1$ and $\bar{\mathbf{C}}^1$ according to the boundary conditions, $\mathbf{x}^q$ is a vector containing the unknown boundary data, and $\mathbf{y}^q$ is a vector containing the prescribed boundary quantities f^*_α and u^*_α. From Eq. (70), the following time-stepping scheme is obtained:

$$\mathbf{x}^q = (\bar{\mathbf{B}}^1)^{-1}\left[\bar{\mathbf{D}}^1\mathbf{y}^q + \sum_{s=1}^{q-1}(\bar{\mathbf{C}}^{q-s+1}\mathbf{f}^s - \bar{\mathbf{A}}^{q-s+1}\mathbf{v}^s)\right] \quad (q = 1, 2, \ldots, N), \tag{71}$$

where $\bar{\mathbf{B}}^1$ is the system matrix at the first time-step and $(\bar{\mathbf{B}}^1)^{-1}$ is its inverse. Eq. (71) implies that that at each time-step only two new system matrices $\bar{\mathbf{C}}^{q-s+1}$ and $\bar{\mathbf{A}}^{q-s+1}$ have to be computed. By using the time-stepping scheme (71), the unknown CODs and other boundary data can be determined numerically step by step.

4. Computation of dynamic stress intensity factors

Once the CODs have been computed numerically by the time-stepping scheme as presented in the last section, the Mode-I and the Mode-II dynamic stress intensity factors can be obtained by using the following relations:

$$\begin{Bmatrix} K_{\mathrm{I}}(t) \\ K_{\mathrm{II}}(t) \end{Bmatrix} = \frac{\mu\sqrt{2\pi}}{4(1-\nu)} \lim_{\delta\to 0} \frac{1}{\sqrt{\delta}} \begin{Bmatrix} \Delta u_\zeta(\delta, t) \\ \Delta u_\xi(\delta, t) \end{Bmatrix} \tag{72}$$

where ν denotes Poisson's ratio and δ is the distance from the midpoint (collocation point) of the "crack-tip element" to the crack-tip considered. Also, ξ and ζ are the local coordinates centered at the crack-tip, with ξ tangential and ζ normal to the crack-faces.

The dynamic stress intensity factors represent the strength of the inverse square-root singularity of the stress field at a crack-tip and they are the most important crack-tip characterizing parameters in linear elastic fracture mechanics. The displacements and the stresses at an arbitrary interior domain point can be obtained by using the representation formula (10) and Hooke's law (2).

5. Numerical examples

To show the efficiency and the accuracy of the hypersingular time-domain traction BEM presented here, several numerical examples are given in this section. For convenience, the dynamic stress intensity factors are normalized

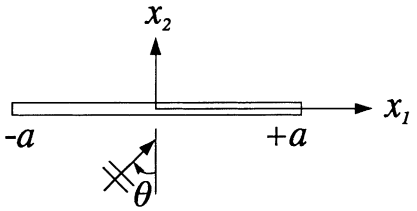

Fig. 3. A finite crack in an infinite elastic solid.

by

$$\bar{K}_i(t) = \frac{K_i(t)}{K_i^{\mathrm{st}}}, \quad (i = \mathrm{I}, \mathrm{II}), \tag{73}$$

where $K_{\mathrm{I}}^{\mathrm{st}} = \sigma_{22}\sqrt{\pi a}$ and $K_{\mathrm{II}}^{\mathrm{st}} = \sigma_{12}\sqrt{\pi a}$ are the corresponding static stress intensity factors for an infinite solid containing a central crack of length $2a$ subject to remote static stresses σ_{22} and σ_{12} at infinity.

5.1. Infinite solids with a finite crack

A finite crack of length $2a$ contained in an infinite elastic solid as shown in Fig. 3 is first considered. Poisson's ratio is taken as $\nu = 0.25$ and plane strain condition is assumed. Transient plane longitudinal (L-) and transverse (TV-) elastic waves are supposed as external loading. For a plane L-wave, the incident displacement field is given by

$$u_i^{\mathrm{in}} = U_{\mathrm{L}} \begin{Bmatrix} \sin\theta \\ \cos\theta \end{Bmatrix} [c_{\mathrm{L}}t - (x_1 + a)\sin\theta - x_2\cos\theta] \times H[c_{\mathrm{L}}t - (x_1 + a)\sin\theta - x_2\cos\theta], \tag{74}$$

while for a plane TV-wave the incident displacement field is described by

$$u_i^{\mathrm{in}} = U_{\mathrm{T}} \begin{Bmatrix} -\cos\theta \\ \sin\theta \end{Bmatrix} [c_{\mathrm{T}}t - (x_1 + a)\sin\theta - x_2\cos\theta] \times H[c_{\mathrm{T}}t - (x_1 + a)\sin\theta - x_2\cos\theta]. \tag{75}$$

In Eqs. (74) and (75), U_{L} and U_{T} are displacement amplitudes of the incident L- and TV-waves, θ is the incidence angle, and $H[\cdot]$ is the Heaviside step function, respectively. The corresponding incident stress field can be obtained by substituting Eqs. (74) and (75) into Hooke's law (2). A total number of 20 elements has been used for the discretization of the crack-face and a time-step $\Delta t = 0.1a/c_{\mathrm{T}}$ is applied. This time-step corresponds to a time needed by a TV-wave to travel one element-length.

For an incidence of transient plane L-waves with several values of incidence angle θ, the normalized Mode-I and Mode-II dynamic stress intensity factors are presented in Figs. 4 and 5. Here, the superscript "$\pm$" designates the left and the right crack-tip. The analytical results obtained by Thau and Lu [30] for $\theta = 0^\circ$ and $\theta = 30^\circ$ are also given in Figs. 4(a) and 5(a) and (b) for comparison purpose. Thau and Lu [30] applied a Wiener–Hopf technique for solving their singular integral equations and they could obtain analytical solutions in the small-time range. By the comparison it can be seen that the present results agree very well with the analytical results of Thau and Lu [30]. A mesh refinement in the spatial discretization by using 40 elements will improve the agreement between both results near the peaks in the normalized dynamic stress intensity factors, but no essential qualitative differences were obtained. Thau and Lu [30] could show that the peaks appear at the time which is needed by a Rayleigh wave to travel from one crack-tip to another. The maximum dynamic overshoot of the dynamic stress intensity factors is 30% over their corresponding static values. For normal ($\theta = 0^\circ$) and grazing ($\theta = 90^\circ$) incidence of plane L-waves, the Mode-II dynamic stress intensity factors vanish, since no shear stress component on the crack-faces is

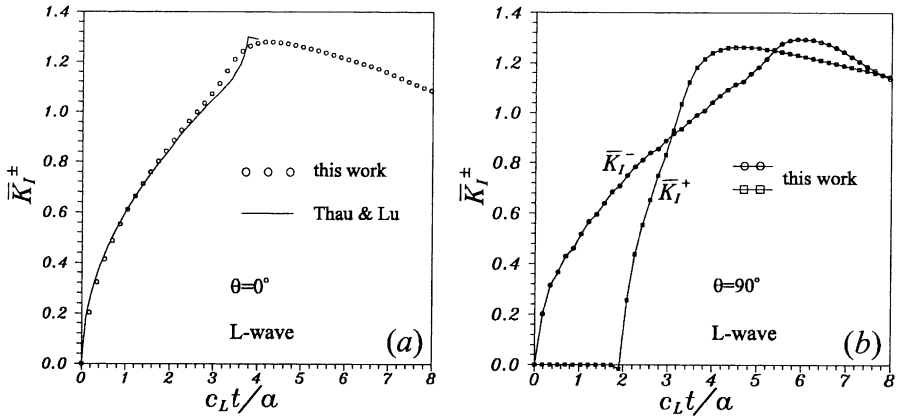

Fig. 4. $\bar{K}_{\mathrm{I}}^{\pm}$-factors for normal ($\theta = 0^{\circ}$) and grazing ($\theta = 90^{\circ}$) incidence of L-waves.

induced in these cases. The dynamic stress intensity factors for $\theta \neq 0^{\circ}$ and $\theta \neq 30^{\circ}$ presented here are not reported elsewhere in literature, to the author's knowledge.

The corresponding normalized dynamic stress intensity factors for incident transient plane elastic TV-waves are shown in Figs. 6 and 7, versus the dimensionless time $c_{\mathrm{L}}t/a$. The analytical result of Thau and Lu [30] for normal incidence, i.e. $\theta = 0^{\circ}$, is also given in Fig. 6(a). Here again, very good agreement between both results is achieved. For normal and grazing incidence of plane TV-waves, no stress component normal to the crack-faces is induced, and the Mode-I dynamic stress intensity factors $K_{\mathrm{I}}^{\pm}$ are hence identically zero. In contrast, no shear stress component on the crack-faces is produced by an incident plane TV-wave under an incidence angle $\theta = 45^{\circ}$, and the corresponding Mode-II dynamic stress intensity factors $K_{\mathrm{II}}^{\pm}$ are therefore zero. In other cases, both the Mode-I and the Mode-II dynamic stress intensity factors are nonzero once the front of the incident wave which arrives at the crack-tip is considered. Similar to the case of incident plane L-waves, the dynamic stress intensity factors may exceed their corresponding static values by maximum 30%. The dynamic stress intensity factors induced by an incident plane TV-wave with $\theta \neq 0^{\circ}$ are not reported in literature, and they are given here for the purpose of completeness.

In the long-time limit, the dynamic stress intensity factors should approach their corresponding static values, i.e., $\bar{K}_{\mathrm{I}}^{\pm}(t \to \infty) = \bar{K}_{\mathrm{II}}^{\pm}(t \to \infty) = 1$. This long-time limit has been used as an additional check for the present numerical solution procedure. In all cases considered here, the deviation between the numerical results and the exact results in the long-time limit is about 3%.

5.2. Bounded solids with a crack

In the following, some numerical results for bounded solids with a crack obtained by the present hypersingular time-domain traction BEM are given.

First, we consider a rectangular plate with an inclined edge crack in 2D plane strain as shown in Fig. 8. The inclination angle of the crack with respect to the horizontal plate boundary is 45°. The material and the geometrical data used for the numerical computations are also given in Fig. 8. The plate is subjected to an impact loading on its upper boundary. Mixed boundary conditions are supplied on other plate boundaries, with a fixed constraint normal to the boundaries and an allowance for tangential movements.

A total number of 87 elements have been used for discretizing the external plate boundaries and the crack-face: 11 for the crack-face, 32 for the horizontal plate boundaries, and 44 for the vertical plate boundaries. The time-step is taken as $\Delta t = (B/32)/c_{\mathrm{L}} = 0.15804\,\mu\mathrm{s}$ where B is the plate width.

Fig. 9 shows the normalized dynamic stress intensity factors $\bar{K}_{\mathrm{I}}(t)$ and $\bar{K}_{\mathrm{II}}(t)$ versus time t. The numerical results obtained by Domínguez and Gallego [11] via time-domain displacement BEM in conjunction with

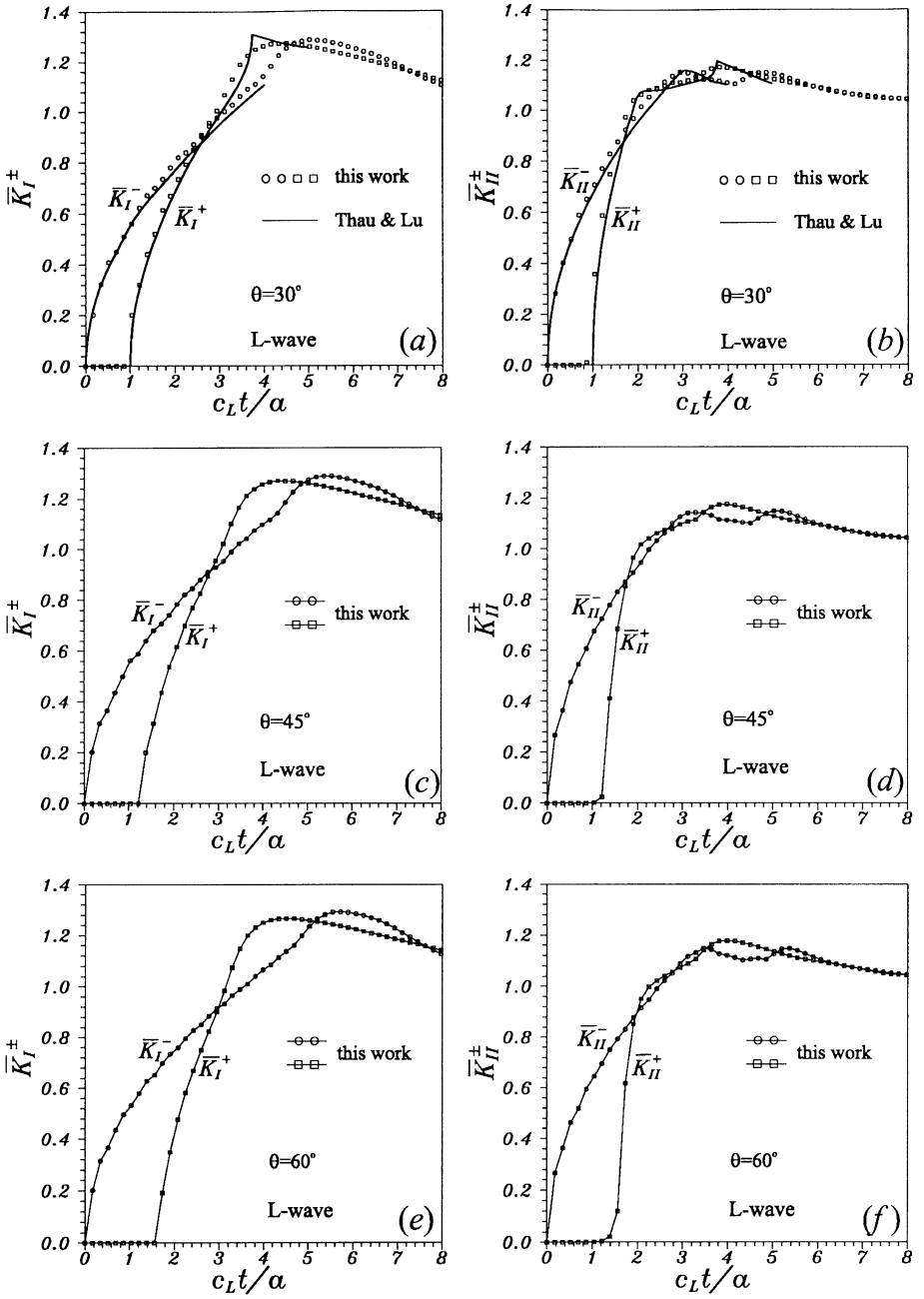

Fig. 5. $\bar{K}_{\mathrm{I}}^{\pm}$- and $\bar{K}_{\mathrm{II}}^{\pm}$-factors for oblique incidence of L-waves.

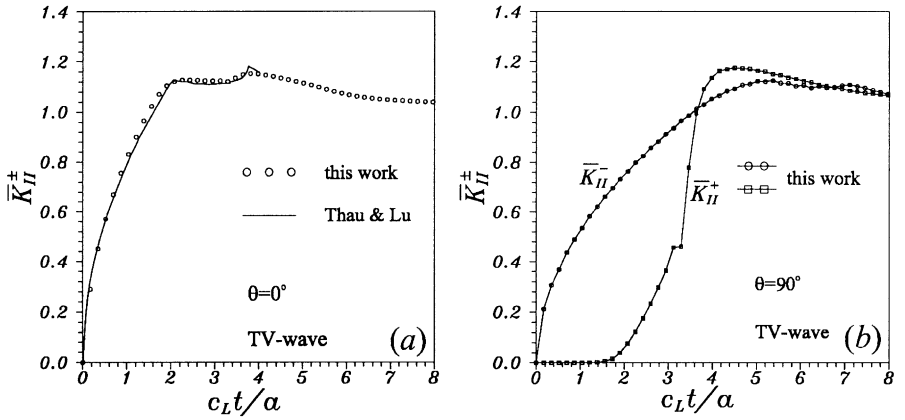

Fig. 6. $\bar{K}_{\mathrm{II}}^{\pm}$-factors for normal ($\theta = 0^{\circ}$) and grazing ($\theta = 90^{\circ}$) incidence of TV-waves.

domain-substructuring by Fedelinski et al. [14] via Laplace transform dual BEM, and by Murti and Valliappan [18] via finite element method are also given in Fig. 9. Fig. 9 shows that the present numerical results agree very well with that of other authors, especially in the small-time range. The discrepancy between different numerical results in the large-time range could be caused by different time-steps and techniques applied for evaluating the dynamic stress intensity factors.

Next, we consider a rectangular plate with a central crack of length $2a$ subject to a uniform impact loading normal to the crack-face as shown in Fig. 10. Due to symmetry, it is sufficient to consider the right-half of the cracked plate only, supplemented by proper symmetry conditions. The material constants and the geometrical data used in the numerical calculations are given in Fig. 10. Note here that the material constants applied in this example are the same as in the previous example.

The cracked plate is discretized by 98 elements: 6 for the crack-face, 52 for the horizontal boundaries, and 40 for the vertical boundaries. The time-step is chosen as $\Delta t = (B/52)/c_{\mathrm{L}} = 0.31608\,\mu\mathrm{s}$. The normalized Mode-I dynamic stress factor $\bar{K}_{\mathrm{I}}(t)$ versus time t is presented in Fig. 11. For comparison purpose, the numerical results obtained by Fedelinski et al. [14], Nishioka and Atluri [20], and Murti and Valliappan [18] are also given in Fig. 11. Finite element methods have been used by Nishioka and Atluri [20] as well as Murti and Valliappan [18], while Fedelinski et al. [14] have applied Laplace transform dual BEM. In the small-time range, the present numerical results agree very well with that obtained by other authors. For large time t, the agreement between different numerical results is still quite satisfactory. It should be noted here that the Mode-II dynamic stress intensity factor $\bar{K}_{\mathrm{II}}(t)$ is zero due to symmetry of the problem considered.

Finally, a rectangular plate with an edge crack parallel to the horizontal plate boundaries is investigated, see Fig. 12. The material constants used here are identical to those in the previous examples, and the geometrical data correspond to that of the right-half of the rectangular plate with a central crack as shown in Fig. 10. Thus, the same temporal and spatial discretizations as for the central crack problem treated before have been applied. The cracked plate is subjected to either uniform tension or variable tension and compression corresponding to a bending moment. Numerical results for the normalized dynamic stress intensity factor $\bar{K}_{\mathrm{II}}(t)$ are shown in Fig. 13. This figure implies that with an equal loading amplitude σ^{*}, a constant uniform tension gives rise to a larger dynamic overshoot of the stress intensity factor. The instant, at which the maximum dynamic stress intensity factor appears, is nearly the same for both loading conditions. Here again, the Mode-II dynamic stress intensity factor $\bar{K}_{\mathrm{II}}(t)$ vanishes due to symmetry of the problem.

The numerical results for bounded cracked solids presented here have been obtained by using a linear temporal shape-function for boundary tractions. For the purpose of comparison, a constant temporal shape-function for boundary tractions has also been applied. The present investigation has shown that there are no essential differences

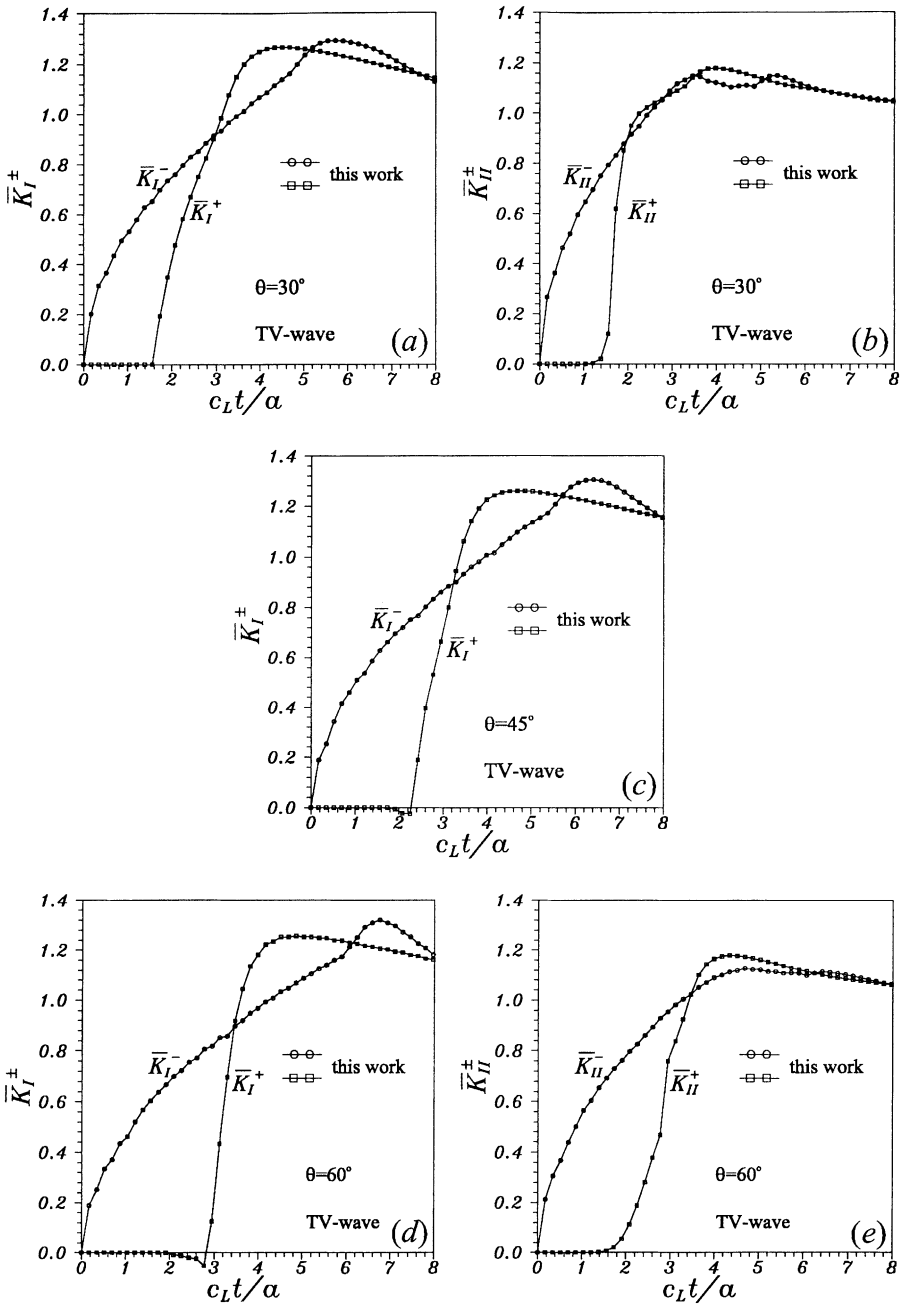

Fig. 7. $\bar{K}_{\mathrm{I}}^{\pm}$- and $\bar{K}_{\mathrm{II}}^{\pm}$-factors for oblique incidence of TV-waves.

between the numerically computed dynamic stress intensity factors obtained by using linear and constant temporal shape-functions for boundary tractions. In literature, it was reported [10] that the combination of a linear temporal shape-function for boundary displacements and a constant temporal shape-function for boundary tractions would be a better choice. This statement cannot be verified by the present investigation, as long as the computation of the

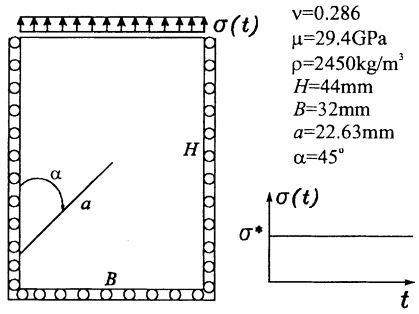

Fig. 8. Rectangular plate with an inclined edge crack.

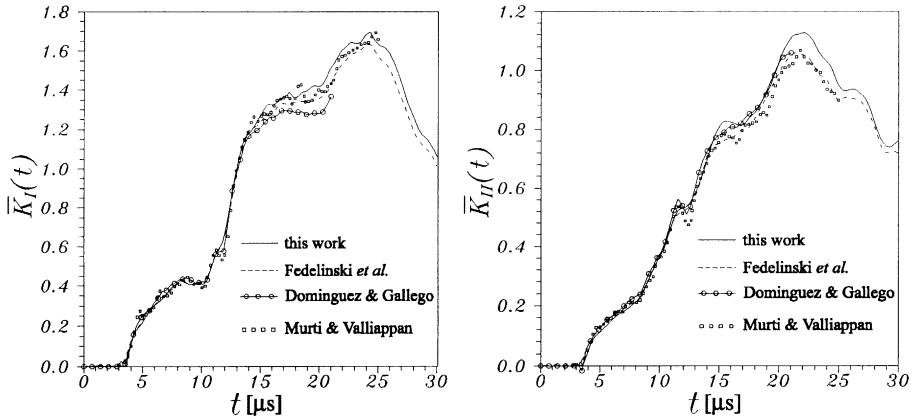

Fig. 9. Normalized $\bar{K}_{\mathrm{I}}$- and $\bar{K}_{\mathrm{II}}$-factors.

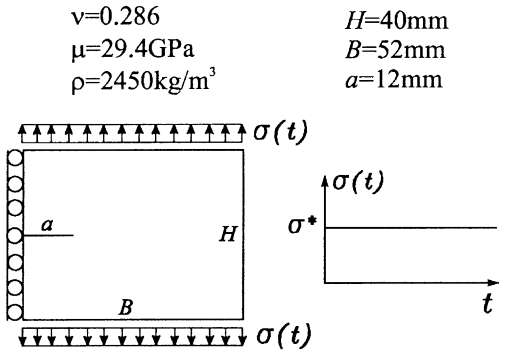

Fig. 10. Rectangular plate with a central crack.

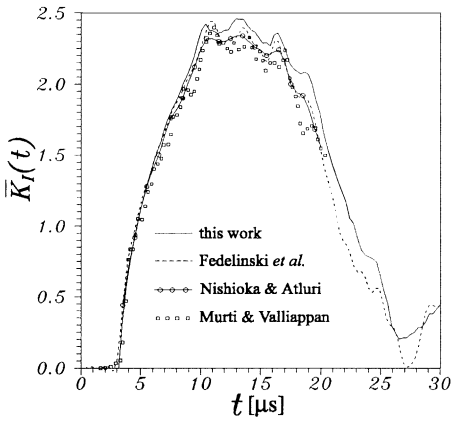

Fig. 11. Normalized $\bar{K}_{\mathrm{I}}$-factor.

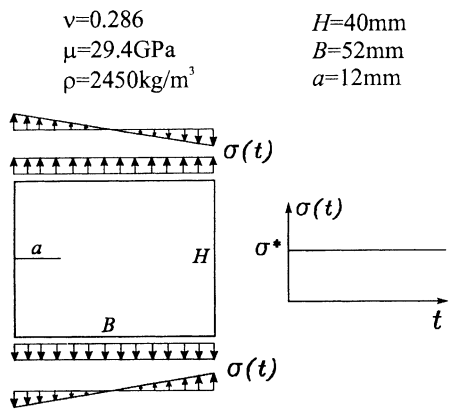

Fig. 12. Rectangular plate with a horizontal edge crack.

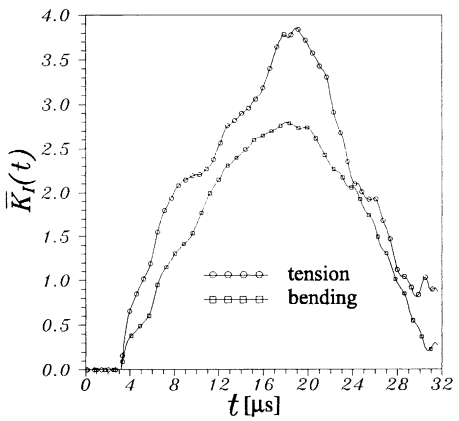

Fig. 13. Normalized $\bar{K}_{\mathrm{II}}$-factor.

dynamic stress intensity factors is concerned. Previous works of Fedelinski [15] support this conclusion who used a time-domain dual BEM for transient dynamic crack analysis of bounded solids.

6. Conclusions

A 2D hypersingular time-domain traction BEM for transient elastodynamic crack analysis is presented in this paper. Unlike the displacement, dual, or combined displacement/traction BEM, the present method applies hypersingular time-domain traction BIEs to both crack-faces and external boundaries of the cracked solids. Linear temporal shape-function is adopted for CODs, boundary displacements, and boundary tractions. For simplicity, constant spatial shape-function is applied for CODs away from crack-tips, boundary displacements and boundary tractions, while a square-root crack-tip shape-function is used for elements adjacent to crack-tips. This enables us to take the proper local behavior of the CODs at crack-tips into account, and to compute the dynamic stress intensity factors from the CODs accurately. The method is very efficient and suitable for transient elastodynamic crack analysis of unbounded and bounded solids. Numerical examples show that the present hypersingular time-domain traction BEM can provide very accurate numerical results for the computation of dynamic stress intensity factors.

Like the commonly applied time-stepping scheme in time-domain displacement and dual BEM, an essential drawback of the present method lies in the critical choice of the time-step. The stability and quality of the numerical results could be drastically affected by the used time-step. A too small time-step may cause an instability of the numerical scheme, while a too large time-step may lead to unreasonable numerical damping of the results. The spatial approximation of the CODs and other boundary data can be improved by using higher order such as isoparametric quadratic shape-functions. This refinement does not, however, significantly improve the stability of the time-stepping scheme in the large-time range.

Appendix A. 2D time-domain Green's functions

Time-domain elastodynamic Green's functions are solutions of the following partial differential equations:

$$\sigma^{\mathrm{G}}_{\alpha\beta\gamma,\beta} - \rho\ddot{u}^{\mathrm{G}}_{\alpha\gamma} = -\delta(t-\tau)\delta(\mathbf{x}-\mathbf{y})\delta_{\alpha\gamma}. \tag{A.1}$$

In 2D case, time-domain Green's functions are given by [1,12,17]

$$u^{\mathrm{G}}_{\alpha\gamma} = \frac{c_{\mathrm{T}}}{2\pi\mu r^2}\left\{\frac{1}{\kappa}H(c_{\mathrm{L}}t'-r)\left[\frac{2(c_{\mathrm{L}}t')^2-r^2}{R_{\mathrm{L}}}r_{,\alpha}r_{,\gamma} - R_{\mathrm{L}}\delta_{\alpha\gamma}\right]\right.$$
$$\left. - H(c_{\mathrm{T}}t'-r)\left[\frac{2(c_{\mathrm{T}}t')^2-r^2}{R_{\mathrm{T}}}r_{,\alpha}r_{,\gamma} - \frac{(c_{\mathrm{T}}t')^2}{R_{\mathrm{T}}}\delta_{\alpha\gamma}\right]\right\}, \tag{A.2}$$

$$\sigma^{\mathrm{G}}_{\alpha\beta\gamma} = E_{\alpha\beta\delta\lambda}\frac{\partial u^{\mathrm{G}}_{\delta\gamma}}{\partial y_\lambda} = \frac{1}{2\pi r^3}\left\{\frac{1}{\kappa}H(c_{\mathrm{L}}t'-r)\left[\frac{2(c_{\mathrm{L}}t')^2-r^2}{R_{\mathrm{L}}}A_{\alpha\beta\gamma} + \frac{r^4}{R_{\mathrm{L}}^3}B^{\mathrm{L}}_{\alpha\beta\gamma}\right]\right.$$
$$\left. - H(c_{\mathrm{T}}t'-r)\left[\frac{2(c_{\mathrm{T}}t')^2-r^2}{R_{\mathrm{T}}}A_{\alpha\beta\gamma} + \frac{r^4}{R_{\mathrm{T}}^3}B^{\mathrm{T}}_{\alpha\beta\gamma}\right]\right\}, \tag{A.3}$$

$$U^{\mathrm{G}}_{\gamma\alpha\beta} = E_{\alpha\beta\delta\lambda}\frac{\partial u^{\mathrm{G}}_{\delta\gamma}}{\partial x_\lambda} = -E_{\alpha\beta\delta\lambda}\frac{\partial u^{\mathrm{G}}_{\delta\gamma}}{\partial y_\lambda} = -\sigma^{\mathrm{G}}_{\alpha\beta\gamma}, \tag{A.4}$$

$$T^{\mathrm{G}}_{\gamma\alpha\beta} = E_{\alpha\beta\delta\lambda}\frac{\partial\sigma^{\mathrm{G}}_{\gamma\eta\delta}}{\partial x_\lambda}n_\eta = \frac{\mu c_{\mathrm{T}}}{2\pi r^2}\left\{\frac{1}{\kappa}H(c_{\mathrm{L}}t'-r)\left[\frac{2(c_{\mathrm{L}}t')^2-r^2}{R_{\mathrm{L}}}\left(\frac{4}{r^2}\right)C_{\gamma\alpha\beta}-\frac{3r^4}{R^5_{\mathrm{L}}}D^{\mathrm{L}}_{\gamma\alpha\beta}+\frac{2r^2}{R^3_{\mathrm{L}}}E^{\mathrm{L}}_{\gamma\alpha\beta}\right]\right.$$
$$\left.-H(c_{\mathrm{T}}t'-r)\left[\frac{2(c_{\mathrm{T}}t')^2-r^2}{R_{\mathrm{T}}}\left(\frac{4}{r^2}\right)C_{\gamma\alpha\beta}-\frac{3r^4}{R^5_{\mathrm{T}}}D^{\mathrm{T}}_{\gamma\alpha\beta}+\frac{2r^2}{R^3_{\mathrm{T}}}E^{\mathrm{T}}_{\gamma\alpha\beta}\right]\right\}, \tag{A.5}$$

where

$$t' = t-\tau, \qquad R_\xi = \sqrt{(c_\xi t')^2-r^2}, \quad \xi = \mathrm{L},\mathrm{T}, \tag{A.6}$$

$$A_{\alpha\beta\gamma} = 2(\delta_{\alpha\beta}r_{,\gamma}+\delta_{\beta\gamma}r_{,\alpha}+\delta_{\alpha\gamma}r_{,\beta}-4r_{,\alpha}r_{,\beta}r_{,\gamma}), \tag{A.7}$$

$$B^{\mathrm{L}}_{\alpha\beta\gamma} = (\kappa^2-2)\delta_{\alpha\beta}r_{,\gamma}+2r_{,\alpha}r_{,\beta}r_{,\gamma}, \tag{A.8}$$

$$B^{\mathrm{T}}_{\alpha\beta\gamma} = 2r_{,\alpha}r_{,\beta}r_{,\gamma}-\delta_{\alpha\gamma}r_{,\beta}-\delta_{\beta\gamma}r_{,\alpha}, \tag{A.9}$$

$$C_{\gamma\alpha\beta} = (4r_{,\alpha}r_{,\beta}-\delta_{\alpha\beta})n_\gamma+(4r_{,\gamma}r_{,\beta}-\delta_{\gamma\beta})n_\alpha+(4r_{,\gamma}r_{,\alpha}-\delta_{\gamma\alpha})n_\beta+4(\delta_{\alpha\beta}r_{,\gamma}+\delta_{\gamma\beta}r_{,\alpha}$$
$$+\delta_{\gamma\alpha}r_{,\beta}-6r_{,\gamma}r_{,\alpha}r_{,\beta})r_{,\lambda}n_\lambda, \tag{A.10}$$

$$D^{\mathrm{L}}_{\gamma\alpha\beta} = [(\kappa^2-2)n_\gamma+2r_{,\gamma}r_{,\lambda}n_\lambda][(\kappa^2-2)\delta_{\alpha\beta}+2r_{,\alpha}r_{,\beta}], \tag{A.11}$$

$$D^{\mathrm{T}}_{\gamma\alpha\beta} = (4r_{,\gamma}r_{,\alpha}r_{,\beta}-\delta_{\gamma\beta}r_{,\alpha}-\delta_{\gamma\alpha}r_{,\beta})r_{,\lambda}n_\lambda-r_{,\gamma}r_{,\alpha}n_\beta-r_{,\gamma}r_{,\beta}n_\alpha, \tag{A.12}$$

$$E^{\mathrm{L}}_{\gamma\alpha\beta} = -[\kappa^2(\kappa^2-2)\delta_{\alpha\beta}+2r_{,\alpha}r_{,\beta}]n_\gamma-2r_{,\gamma}r_{,\beta}n_\alpha-2r_{,\gamma}r_{,\alpha}n_\beta$$
$$-2(\delta_{\alpha\beta}r_{,\gamma}+\delta_{\beta\gamma}r_{,\alpha}+\delta_{\alpha\gamma}r_{,\beta}-6r_{,\gamma}r_{,\alpha}r_{,\beta})r_{,\lambda}n_\lambda, \tag{A.13}$$

$$E^{\mathrm{T}}_{\gamma\alpha\beta} = (\delta_{\gamma\beta}-2r_{,\gamma}r_{,\beta})n_\alpha+(\delta_{\gamma\alpha}-2r_{,\gamma}r_{,\alpha})n_\beta-2r_{,\alpha}r_{,\beta}n_\gamma$$
$$-2(\delta_{\alpha\beta}r_{,\gamma}+\delta_{\gamma\beta}r_{,\alpha}+\delta_{\gamma\alpha}r_{,\beta}-6r_{,\gamma}r_{,\alpha}r_{,\beta})r_{,\lambda}n_\lambda. \tag{A.14}$$

Physically, the displacement Green's function $u^{\mathrm{G}}_{\alpha\gamma}(\mathbf{x},t;\mathbf{y},\tau)$ represents the displacement in the α-direction at position $\mathbf{y}$ and time t caused by a unit point-force in the γ-direction and applied at position $\mathbf{x}$ and time τ.

The displacement Green's function has the following properties:

1. *Causality*:

$$u^{\mathrm{G}}_{\alpha\gamma}(\mathbf{x},t;\mathbf{y},\tau) = 0 \quad \text{if } c_{\mathrm{L}}t \le r. \tag{A.15}$$

2. *Invariance of time-translation*:

$$u^{\mathrm{G}}_{\alpha\gamma}(\mathbf{x},t+t^*;\mathbf{y},\tau+t^*) = u^{\mathrm{G}}_{\alpha\gamma}(\mathbf{x},t;\mathbf{y},\tau). \tag{A.16}$$

Appendix B. Auxiliary functions

The auxiliary functions arising in the system matrices $A^{mn}_{\gamma\alpha;ed}$, $B^{mn}_{\gamma\alpha;ed}$ and $C^{mn}_{\gamma\alpha;ed}$ in the case of $\mathbf{x}_d \in \Gamma_e$ are given by

$$C_{\gamma\alpha\beta}n_\beta = -2n_\gamma n_\alpha-\delta_{\gamma\alpha}+4r_{,\gamma}r_{,\alpha}, \tag{B.1}$$

$$D^{\mathrm{L}}_{\gamma\alpha\beta}n_\beta = (\kappa^2-2)^2 n_\gamma n_\alpha, \tag{B.2}$$

$$D^{\mathrm{T}}_{\gamma\alpha\beta}n_\beta = -r_{,\gamma}r_{,\alpha}, \tag{B.3}$$

$$E^{\mathrm{L}}_{\gamma\alpha\beta}n_\beta = -\kappa^2(\kappa^2-2)n_\gamma n_\alpha - 2r_{,\gamma}r_{,\alpha}, \tag{B.4}$$

$$E^{\mathrm{T}}_{\gamma\alpha\beta}n_\beta = n_\gamma n_\alpha + \delta_{\gamma\alpha} - 2r_{,\gamma}r_{,\alpha}. \tag{B.5}$$

By using the relations of Eq. (40), it can be easily shown that the above auxiliary functions are independent of the local coordinate or integration variable η.

Appendix C. Evaluation of CPV and HFP integrals

The strongly singular CPV integral and the hypersingular HFP integral can be written as

$$I_1 = \int_{-1}^{+1} \frac{1}{\eta-\eta^*} g(\eta)\,\mathrm{d}\eta, \tag{C.1}$$

$$I_2 = \int_{-1}^{+1} \frac{1}{(\eta-\eta^*)^2} h(\eta)\,\mathrm{d}\eta, \tag{C.2}$$

where η denotes the local coordinate system, η^* represents the collocation point, and $g(\eta)$ and $h(\eta)$ are regular functions. The integrals (C.1) and (C.2) can be rewritten as

$$I_1 = \int_{-1}^{+1} \frac{1}{\eta-\eta^*}[g(\eta)-g(\eta^*)]\,\mathrm{d}\eta + g(\eta^*)\int_{-1}^{+1}\frac{1}{\eta-\eta^*}\,\mathrm{d}\eta, \tag{C.3}$$

$$\begin{aligned} I_2 = {} & \int_{-1}^{+1} \frac{1}{(\eta-\eta^*)^2}\left[h(\eta)-h(\eta^*)-(\eta-\eta^*)\left.\frac{\partial h}{\partial\eta}\right|_{\eta=\eta^*}\right]\mathrm{d}\eta \\ & + h(\eta^*)\int_{-1}^{+1}\frac{1}{(\eta-\eta^*)^2}\,\mathrm{d}\eta + \left.\frac{\partial h}{\partial\eta}\right|_{\eta=\eta^*}\int_{-1}^{+1}\frac{1}{\eta-\eta^*}\,\mathrm{d}\eta. \end{aligned} \tag{C.4}$$

Assuming that $g(\eta)$, $h(\eta)$ and $\partial h/\partial\eta$ satisfy Hölder continuity condition at $\eta=\eta^*$, the first integrals in Eqs. (C.1) and (C.2) are regular since

$$[g(\eta)-g(\eta^*)] \propto (\eta-\eta^*), \tag{C.5}$$

$$\left[h(\eta)-h(\eta^*)-(\eta-\eta^*)\left.\frac{\partial h}{\partial\eta}\right|_{\eta=\eta^*}\right] \propto (\eta-\eta^*)^2. \tag{C.6}$$

Hence, the integration of the first integrals in Eqs. (C.3) and (C.4) can be performed numerically by using standard Gaussian quadrature formula. The remaining integrals in Eqs. (C.3) and (C.4) can be evaluated analytically by using the following integration formulas:

$$\int_{-1}^{+1}\frac{1}{\xi-\xi^*}\,\mathrm{d}\xi = \ln\left|\frac{1-\xi^*}{1+\xi^*}\right|, \qquad \int_{-1}^{+1}\frac{1}{(\xi-\xi^*)^2}\,\mathrm{d}\xi = -\frac{2}{1-\xi^{*2}}. \tag{C.7}$$

In literature, this technique is often referred to as the singularity-subtraction method.

References

[1] J.D. Achenbach, Wave Propagation in Elastic Solids, North-Holland, Amsterdam, 1973.
[2] M.H. Aliabadi, D.P. Rooke, Numerical Fracture Mechanics, Computational Mechanics Publications, Southampton, UK, 1991.
[3] M.H. Aliabadi, Boundary element formulations in fracture mechanics, Appl. Mech. Rev. 50 (1997) 83–96.
[4] D. Barbier, Méthode des potentiels retardés pour la simulation de la diffraction d'onde élastodynamique par une fissure tridimensionnelle, Ph.D. Thesis, École Polytecnique, France, 1999.
[5] E. Bécache, A variational boundary integral equation method for an elastodynamic antiplane crack, Int. J. Numer. Meth. Eng. 36 (1993) 969–984.
[6] D.E. Beskos, Boundary element methods in dynamic analysis. Part II (1986–1996), Appl. Mech. Rev. 50 (1997) 149–197.
[7] M. Bonnet, Boundary Integral Equation Methods for Solids and Fluids, Wiley, New York, 1999.
[8] J.T. Chen, Review of dual boundary element methods with emphasis on hypersingular integrals and divergent series, Appl. Mech. Rev. 52 (1999) 17–33, Kluwer Academic Publishers, Boston, MA, 1988.
[9] T.A. Cruse, Boundary Element Analysis in Computational Fracture Mechanics, Kluwer Academic Publishers, Boston, MA, 1988.
[10] J. Domínguez, Boundary Elements in Dynamics, Computational Mechanics Publications, Southampton, UK, 1993.
[11] J. Domínguez, R. Gallego, Time domain boundary element method for dynamic stress intensity factor computations, Int. J. Numer. Meth. Eng. 33 (1992) 635–647.
[12] A.C. Eringen, E.S. Suhubi, Elastodynamics, Vol. II: Linear Theory, Academic Press, New York, 1975.
[13] P. Fedelinski, M.H. Aliabadi, D.P. Rooke, The dual boundary element method in dynamic fracture mechanics, Eng. Anal. Bound. Elem. 12 (1993) 203–210.
[14] P. Fedelinski, M.H. Aliabadi, D.P. Rooke, The Laplace transform DBEM for mixed-mode dynamic crack analysis, Comput. Struct. 59 (1996) 1021–1031.
[15] P. Fedelinski, Private communications, 1999.
[16] R. Gallego, J. Domínguez, Hypersingular BEM for transient elastodynamics, Int. J. Numer. Meth. Eng. 39 (1996) 1681–1705.
[17] A.S.M. Israil, P.K. Banerjee, Interior stress calculations in 2D time-domain transient BEM analysis, Int. J. Solids Struct. 27 (1991) 915–927.
[18] V. Murti, S. Valliappan, The use of quarter point element in dynamic crack analysis, Eng. Fract. Mech. 23 (1986) 585–614.
[19] N. Nishimura, S. Kobayashi, A regularized boundary integral equation method for elastodynamic crack problems, Comput. Mech. 4 (1989) 319–328.
[20] T. Nishioka, S.N. Atluri, Numerical modelling of dynamic propagation in finite bodies by moving singular elements. II. Results, ASME J. Appl. Mech. 47 (1980) 577–582.
[21] J.D. Richardson, T.A. Cruse, Nonsingular BEM for fracture modelling, Comput. Struct. 66 (1998) 695–703.
[22] Th. Seelig, Zur simulation der dynamischen Riausbreitung mit einer Zeitbereichs-Randelementmethode, Ph.D. Thesis, TH Darmstadt, Germany, 1997.
[23] Th. Seelig, D. Gross, Dynamic crack propagation analysis by a boundary integral equation method, in: B.L. Karihaloo, et al. (Eds.), Advances in Fracture Research, ICF 9, Vol. 6, Pergamon Press, Oxford, 1997, pp. 2877–2884.
[24] Th. Seelig, D. Gross, Analysis of dynamic crack propagation using a time-domain boundary integral equation method, Int. J. Solids Struct. 34 (1997) 2087–2103.
[25] V. Sládek, J. Sládek, Transient elastodynamic three-dimensional problems in cracked bodies, Appl. Math. Model. 8 (1984) 2–10.
[26] V. Sládek, J. Sládek, M. Tanaka, Nonsingular BEM formulations for thin-walled structures and elastostatic crack problems, Acta Mech. 99 (1993) 173–190.
[27] V. Sládek, J. Sládek (Eds.), Singular Integrals in Boundary Element Methods, Computational Mechanics Publications, Southampton, UK, 1998.
[28] J. Sládek, V. Sládek, Nonsingular traction BIEs for crack problems in elastodynamics, Comput. Mech. 25 (2000) 590–599.
[29] M. Tanaka, V. Sládek, J. Sládek, Regularization techniques applied to boundary element methods, Appl. Mech. Rev. 47 (1994) 457–499.
[30] S.A. Thau, T.H. Lu, Transient stress intensity factors for a finite crack in an elastic solid caused by a dilatational wave, Int. J. Solids Struct. 7 (1971) 731–750.
[31] Ch. Zhang, J.D. Achenbach, A new boundary integral equation formulation for elastodynamic and elastostatic crack analysis, ASME J. Appl. Mech. 56 (1989) 284–290.
[32] Ch. Zhang, A novel derivation of non-hypersingular time-domain BIEs for transient elastodynamic crack analysis, Int. J. Solids Struct. 28 (1991) 267–281.
[33] Ch. Zhang, D. Gross, A non-hypersingular time-domain BIEM for transient elastodynamic crack analysis, Int. J. Numer. Meth. Eng. 36 (1993) 2997–3017.
[34] Ch. Zhang, D. Gross, On Wave Propagation in Elastic Solids With Cracks, Computational Mechanics Publications, Southampton, UK, 1997.
[35] Ch. Zhang, A. Savaidis, A hypersingular BEM for dynamic crack analysis, ZAMM Z. Angew. Math. Mech. 79 (1999).
[36] Ch. Zhang, A. Savaidis, Time-domain BEM for dynamic crack analysis, Math. Comput. Simulation 50 (1999) 351–362.
[37] Ch. Zhang, A. Savaidis, Dynamic crack analysis by hypersingular and non-hypersingular time-domain BEM, in: Proceedings of the IUTAM/IACM/IABEM Symposium on Mathematical and Computational Mechanics Aspects of the Boundary Element Method, Kluwer Academic Publishers, Dordrecht, in press.